sustainability

MDPI

Article

Experimental Investigation on Performance Enhancement of Parabolic Trough Concentrator with Helical Rotating Shaft Insert

Mohamed Allam [1,2], Mohamed Tawfik [2,*], Maher Bekheit [2] and Emad El-Negiry [2]

[1] Misr International Technological University MITU, Cairo 11725, Egypt
[2] Mechanical Power Engineering Department, Faculty of Engineering, Mansoura University, Mansoura 35516, Egypt
* Correspondence: m_tawfik@mans.edu.eg

Abstract: The parabolic trough collector provides an extensive range of solar heating and electricity production applications in solar power plants. The receiver tube of the parabolic trough collector has a vital role in enhancing its performance by using different inserts inside it. In the present work, outdoor experimental tests were conducted to study the performance of a small-scale parabolic trough collector equipped with a centrally placed rotating helical shaft. Three cases were studied: a parabolic trough collector without helical shaft insert, a parabolic trough collector with stationary helical shaft insert, and a parabolic trough collector with a rotating helical shaft insert. The experiments are performed for different shaft rotational speeds (4, 11, and 21 RPM) and various flow rates (0.5, 1, 1.5, 2, and 2.5 LPM) of water as a heat transfer fluid. The fluid flow and heat transfer parameters (friction factor, Reynolds number, Nusselt number, and thermal enhancement factor) and performance parameters (thermal, overall, and exergetic efficiencies) are studied. The results indicated that the helical shaft insert had increased the required pumping power for the same flow rate. However, the parabolic trough collector thermal performance has enhanced with the shaft rotational speed. For all cases, the parabolic trough collector efficiency increases with the flow rate of the heat transfer fluid, but the percentage enhancement in efficiency decreases. Using a shaft rotational speed of 21 RPM and heat transfer fluid flow rates of 0.5 LPM leads to maximum thermal efficiency enhancement and a maximum friction factor ratio of 46.47% and 7.7 times, respectively, compared to plain tube. A comparison based on the same pumping power (thermal enhancement factor) shows that the maximum enhancement occurs at a flow rate of 1 LPM, and the efficiency enhancement is about 37% at a shaft rotational speed of 21 RPM. From an economic point of view, using a rotating helical shaft produces the lower annual cost of useful heat per kWh.

Keywords: solar concentrator; thermal; inserts; helical rotating shaft; active methods

Citation: Allam, M.; Tawfik, M.; Bekheit, M.; El-Negiry, E. Experimental Investigation on Performance Enhancement of Parabolic Trough Concentrator with Helical Rotating Shaft Insert. *Sustainability* **2022**, *14*, 14667. https://doi.org/10.3390/su142214667

Academic Editors: Pablo García Triviño, Ahmed El Kenawy, Petra-Manuela Schuwerack, Zhongfeng Xu and Mohamed El-Alfy

Received: 16 July 2022
Accepted: 15 August 2022
Published: 8 November 2022

1. Introduction

Fossil fuel consumption still significantly contributes to energy demand worldwide, so pollution and global warming have become critical problems [1]. At the same time, from 2003 to 2030, worldwide energy consumption is expected to grow by 71% [2]. Therefore, researchers try to address this issue using renewable energy sources, which may offer a solution. Solar thermal power is one of the valuable alternatives for reducing fossil fuel use, reducing greenhouse gases, and satisfying human needs. The concentrated solar power (CSP) technology is classified as line focus or point focus based on the receiving mechanism. The line focus systems include linear Fresnel reflectors and the parabolic trough, while the point focus systems include the parabolic dish, solar tower, and beam-down central receivers [3,4].

The most often applied technique in solar plants to produce electricity and in industrial and thermal processes is the parabolic trough collector (PTC) [5,6]. The concentrator and

the receiver tube are significant components of the solar field. The reflector surface of the concentrator reflects solar rays onto the receiving tube, which converts solar power into heat transmitted to the heat transfer fluid (HTF), such as air, water, or oil [7]. The receiver comprises a selective-coated metallic tube to enhance the absorption of solar irradiance. In addition, the entire tube is enveloped with a vacuumed glass tube with an anti-reflective coating to minimize heat loss by convection [8]. The most critical component of the PTC is the receiver tube, whose performance directly reflects the PTC thermal efficiency. The higher surface temperature of the receiver tube is the major problem that leads to uneven temperature distribution over the receiver. Thus, thermal stresses and losses of the receiver tube increase [9]. Therefore, the thermal efficiency decreases. Because of this, researchers have investigated ways to boost the heat transfer rate within the receiver to improve the PTC thermal performance.

Three techniques enhance heat transfer: passive, active, and compound [10]. The first technique is the passive method that does not consume energy, and the heat transfer rate can be augmented by inserting various inserts inside the receiver tube with a particular engineering design or modifying the entire receiver tube surface. The second technique is the active method, such as surface vibration and magnetic fields, which requires external energy to change the path of HTF to improve the heat transfer rate. Finally, the third technique is the compound method, which combines active and passive methods [11,12]. Low cost and simplicity are why different inserts inside the receiver tube make it the most common ordinary technique to improve heat transfer rate [13].

Using inserts inside the receiver tube augments the velocity fluctuation by forcing the flow beside the tube wall to mix within the flow at core regions [7], enhancing the heat transfer coefficient. Such enhancement reduces thermal losses of the receiver tube and temperature gradient, leading to enhanced thermal efficiency [11], while the significant penalty increases the cost of pumping power through the pressure drop increase [14]. Twisted tape, wire coils, porous inserts, fins, cylindrical/rods, rings, and other insert configurations represent the most common inserts [15]. Twisted tapes are the most often used insert to increase the swirling of the HTF flow to boost the thermal performance [16] and have been investigated in studies [17–24], as introduced in the following paragraphs.

Waghole and Shrivastva [17] assessed the influence of twisted tape within a PTC receiver with twisted ratios of 0.577, 1, and 1.732. Water and silver nanofluid were selected as HTFs under Re numbers (500–6000). Their results showed a rise in thermal efficiency, friction factor, and Nu number of 135–205%, 1–1.75 times, and 1.25–2.1 times, respectively, higher than expected by the conventional receiver. Furthermore, the water friction factor and heat transfer coefficient are lower than silver nanofluid of 0–0.1% volume concentration.

Nakhchi et al. [19] experimentally tested the thermal performance within a pipe with twisted tape inserts with double-cut. Water is chosen as the HTF under the Re numbers range (5000–15,000). The friction factors and Nusselt numbers were increased up to 489% and 177.4%, respectively, for pipes fitted with twisted tapes with a cut ratio of 0.90, compared to the typical tube.

Arunachala [20] experimentally analyzed the PTC performance when equipped with twisted tape and using SYLTHERM 800 as an HTF under Re numbers range of 544–1742 and the twisting ratio of 5.2, 4.1, and 2.7; then, they compared the results with an analytical model. Results showed that, at a minimum twisted ratio of 2.7, the maximum thermal efficiency of 40% is achieved, compared to 19.1% for a plain tube, while the thermo-hydraulic efficiency was decreased to 39.7% because of the increase in pressure drop.

Hosseinalipour et al. [21] numerically investigated decreasing temperature differences within a PTC receiver using a twisted tape insert. The investigation considered superheated steam as HTF with a Re number range (10^4–9.79×10^5) and used different twist ratios (2.5, 5, and 10) and various clearance ratios (0, 0.2, 0.3, 0.4, and 1). The results revealed friction factors and Nu number increases of 1.8–4.1 and 1.0–1.7, respectively. Moreover, the temperature differential over the circumference was reduced by 10–45%.

Elton and Arunachala [22] developed a correlation for the Nu number with twisted tape presence and absence. In addition, they used Soltrace to simulate non-uniform solar radiation. THERMINOL VP-1 was considered HTF and a range of Re numbers varying between (2300–2500). They found that the error in the developed correlations for standard and modified tubes lies within a range (±19% and ±20%), respectively.

Ghadirijafarbeigloo et al. [23] numerically investigated twisted louvered tapes and compared the findings with typically twisted tape inserts at various twisting ratios of 2.67, 4, and 5.33. BEHRAN thermal oil was applied as an HTF. In their study, the Re number range was (5000–25,000). They observed that twisted louvered tape had better thermal performance than standard twisted tape. A 210% and 150% increase in friction factor and Nu number was also found when the twisted louvered tape was used.

Song et al. [24] numerically studied using a helical insert and its impact on the PTC receiver thermal performance. First, they employed the Monte Carlo ray-tracing (MCRT) method to model the heat flux distribution over the receiver wall. Next, DOWTHERM-A was considered an HTF within a range of Re number (10,000–75,000) and inlet temperature (373–640 K). They found that at rates of mass flow of 0.11 and 0.6 kg/s, the heat losses were reduced by six and three times, fitting the helical insert. Moreover, a helical screw insert led to a pressure drop increase of 23 times.

Shashank and Sarviya [18] experimentally and numerically investigated the influence of double and single helical inserts with the various twisted ratios of 1.5, 2.5, and 3 inside tubes. They selected water as an HTF with different Re numbers (4000–16,000). They observed that the double-helical insert's Nu number and friction factor were higher than the single helical insert. Moreover, at a low twisted ratio, the maximum enhancement of Nu number was 112% for a double helical insert compared to an empty tube with an average friction factor of 9.1. Finally, the optimum value of entropy production number was achieved for double helical insert compared to single helical insert.

Another method to improve the thermal performance is rotating twisted tapes within the tube. This method was analyzed experimentally by Abdullah et al. [25]. The different twisted tape ratios and variable operating rotational speeds, under constant heat flux with air as HTF and three Re numbers 8000, 10,000, and 13,000. They observed a thermal enhancement for tubes with twisted rotational tape than tubes with fixed insert. Furthermore, the higher twisted tape rotational speed and lower twisted ratio demonstrated improved thermal performance with a higher friction factor.

Cong et al. [26] experimentally studied the flow characteristic and thermal performance of a tube with a stationary twisted tape and a rotating one at 4 RPM with TiO_2-water nanofluid as an HTF. In addition, different Re numbers from 600 to 7000 and different mass fractions of nanoparticles of 0.1%, 0.3%, and 0.5% were studied. They observed that using the applied nanofluid with rotating twisted tape improved the thermal performance by 53.1–101.6%. Furthermore, the exergy efficiency of the stationary twisted tape was increased compared to the plain tube case under similar pumping power. On the other hand, it can be reduced by using the combination of nanofluids and rotating twisted tape.

Pavan et al. [27] investigated experimentally using rotating twisted tape of twisted ratio 2.37 within a tube. Under constant heat flux affecting the tube, water-CuO nanofluid of 0.2% volume concentration was used as HTF for different twisted tape rotational speeds and flow rates. It was concluded that, at a higher rotational speed of 300 RPM, the highest increase in heat transfer coefficient was 347% while using rotating twisted tape and nanofluid together, compared with plain tube, but the friction factor was increased 3.3 times. Other researchers used different types of inserts or compared them to increase the heat transfer performance.

Promvonge [28] experimentally studied thermal performance enhancement in tubes supplied with twisted tapes and wire coils. The applied HTF was the air with Re numbers (3000–18,000) under constant heat flux. The experiment included wire coils with different pitch ratios and twisted tapes with various twist ratios. They observed a double rise in heat transfer when using twisted tapes with wire coils compared to twisted tape or wire

coils. They also observed that using wire coils and twisted tapes with a lower twist ratio and pitch could enhance thermal performance.

Varun et al. [29] compared the PTC performance with a wire matrix and twisted tape. The variable solar irradiance was simulated using the SOLTRACE software program. Two twisted tapes were presented with twisted ratios of 3.37 and 7.86, while three different configurations of wire matrices were presented. The selected HTF was SYNTHETIC oil under the Re number range of 1200–8200 and varying irradiation from 450 to 800 W/m^2. The experimental work showed that the augmentation in thermal efficiency for both twisted tape of 3.37 and medium dense wire matrix were 15.5% and 55.5%, respectively, with a comparable rise in pressure drop of 242% and 3602%, respectively. Regarding performance evaluation criterion analysis, the twisted tape of 3.37 is higher, whereas, in thermo-hydraulic analysis, the medium dense wire matrix is higher.

Other inserts were used to enhance heat transfer; Chakraborty et al. [30] utilized a helical coil within the receiver of a PTC. They simulated the cases using the ANSYS software for pure water mass flow rates (0.016–0.033 kg/s). The exergy and thermal efficiency were increased by 2.4–3.3% and 10–16%, respectively, when helical coils were inserted within the receiver, despite the increased pumping power. Zhao et al. [31] experimentally studied using pin fines within the PTC receiver tube, with air as an HTF for Re number range of 40,000–60,000. It can be concluded from the obtained results that PTC fitted with pin fines enhanced both exergy and energy efficiency by 2.55–4.29% and 10.4–14.5% in comparison with the plain receiver, while the pressure losses were increased about 10–20 times.

The use of metal foam within a PTC receiver was examined experimentally by Jamal-Abad et al. [32] using water as HTF at various Re numbers ranging from 750 to 2000. Results illustrated that using the receiver with metal foam resulted in Nu number and thermal efficiency increase by 1.01–1.80 and 1.03 to 1.08, respectively. Furthermore, the friction factor was intensified. The overall loss coefficient was reduced, which boosted the PTC thermal efficiency. The current study investigates the effect of rotating helical shaft within a PTC receiver using outdoor experimental work with water as HTF. The experimental work is performed for different shaft rotational speeds and flow rates. According to the literature, using a rotating helical shaft inside the PTC receiver as an enhanced insert has not been investigated before. Three cases are compared and studied: a PTC without insert, a PTC with the stationary helical shaft, and a PTC with the rotating helical shaft, to determine the optimum case with better heat transfer performance with a low penalty on pressure drop. The primary criteria for evaluating the examined cases depend on fluid flow, heat transfer, and performance parameters. Finally, an economic analysis is carried out to specify the benefits of the proposed systems from an economic point of view.

2. Materials and Methods

2.1. Experimental Test Rig

The experimental test rig was designed mainly to study the PTC performance with a helical shaft rotating centrally inside the receiver. An experimental test rig of PTC is shown in Figure 1, while its schematic diagram is illustrated in Figure 2. The main elements of the test rig comprise a PTC, a solar tracking mechanism, and measuring instruments.

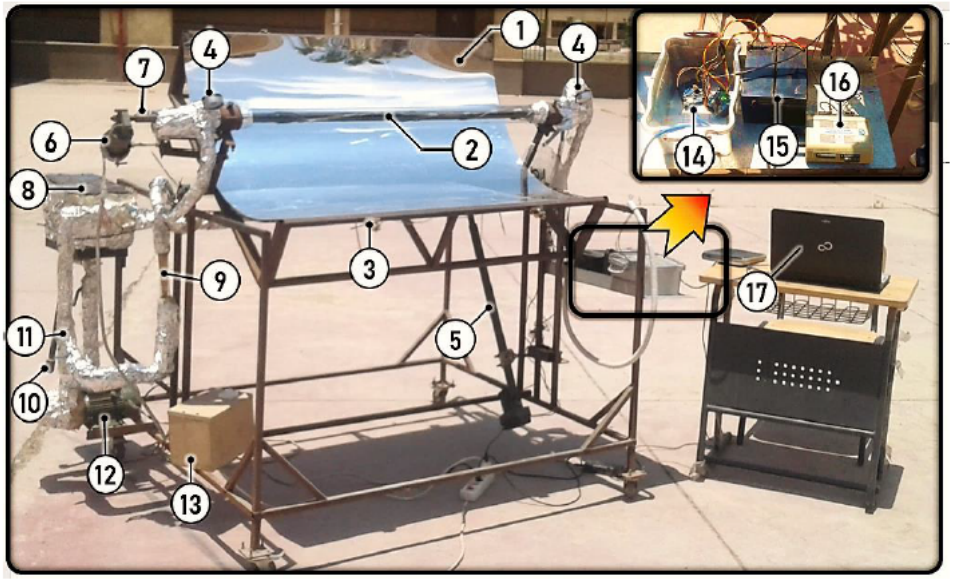

(1) Acrylic reflector sheet	(2) Receiver tube	(3) LDR sensor	(4) Pressure gauge
(5) Linear actuator	(6) DC motor gearbox	(7) Coupling	(8) Storage water tank
(9) Flowmeter	(10) Drain tube	(11) Bypass valve	(12) Circulation pump
(13) DC motor control circuit	(14) ARDUINO circuit	(15) Batteries	(16) Data logger
(17) Laptop			

Figure 1. Experimental test rig of PTC.

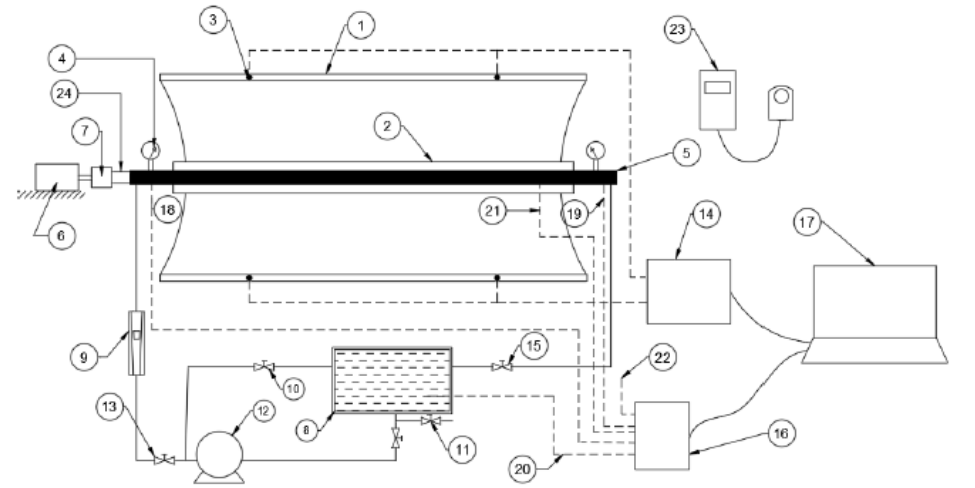

(1) Acrylic reflector sheet	(2) Glass tube	(3) LDR sensor	(4) Pressure gauge
(5) Copper tube	(6) DC motor gearbox	(7) Coupling	(8) Storage water tank
(9) Flowmeter	(10) Bypass valve	(11) Drain valve	(12) Circulation pump
(13) Flow control valve	(14) ARDUINO circuit	(15) Exit valve	(16) Data logger
(17) Laptop	(18) Inlet temperature sensor	(19) Outlet temperature sensor	(20) Inside tank temperature sensor
(21) Temperature sensors (T1-T16)	(22) Ambient temperature sensor	(23) Solar power meter	(24) Helical shaft

Figure 2. The experimental test rig schematic diagram.

2.1.1. Parabolic Trough Solar Collector

The PTC comprises two main components, reflector and receiver.

The Reflector

A 2-mm-thick acrylic mirror sheet was used as a reflector, which can resist outdoor conditions, including heat, cold, and dampness, besides their lightweight and easy to fabricate. The solar-weighted spectral reflectance was tested using a JASCO V-570 Spectrophotometer. The results are plotted in Figure 3, which indicates an average solar weighted solar reflectance of 0.84. The reflector was designed in a parabola shape using two parameters of aperture width (W) and focal distance (F), as shown in Figure 4. The reflector sheet was fixed onto a 1.5-mm-thick steel sheet attached to three steel ribs to increase resistance against the wind load.

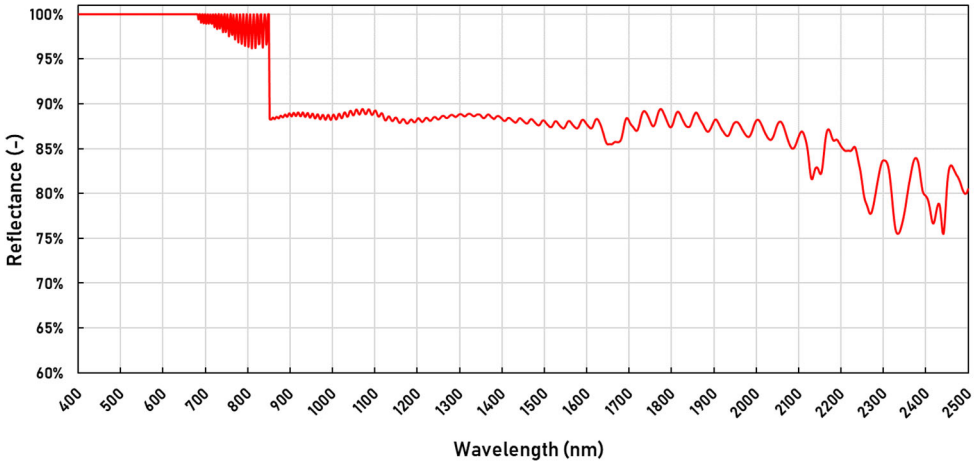

Figure 3. The spectral reflectance of the acrylic mirror sheet.

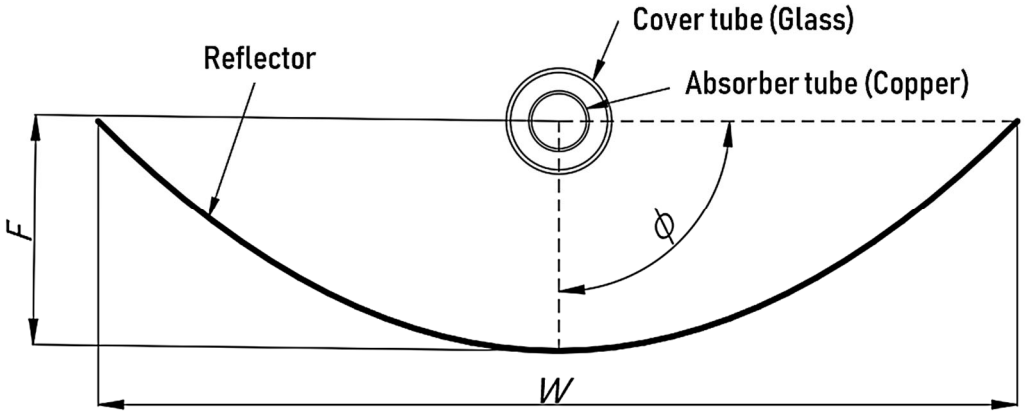

Figure 4. The characteristic dimensions of the tested PTC.

The width of the aperture, W, of the parabola and its focal length, F, are determined using the following Equations [33,34]:

$$W = \frac{2\ Stan(0.5\phi)}{[sec(0.5\phi) + tan(0.5\phi) + ln(sec(0.5\phi) + tan(0.5\phi))]} \quad (1)$$

$$F = \frac{W}{4\ tan(0.5\phi)} \quad (2)$$

where ϕ is the rim angle, and S is the acrylic mirror width (arc length). The following equations were used to assess the correctness of the parabola drawing [35]:

$$y = \frac{x^2}{4F} \quad (3)$$

The concentration ratio, C, representing the concentrator aperture area to the receiver areas, is given by [36,37]:

$$C = \frac{W}{\pi D_o} \tag{4}$$

Specifications of the reflector are provided in Table 1

Table 1. Specification of the reflector.

Parameter	Value
Aperture width, W	0.871 m
The parabolic trough length, L	1.200 m
Aperture area, A_a	1.050 m^2
Rim angle, ϕ	90°
Focal line distance, F	0.218 m
wide of mirror acrylic sheet, S	1.000 m
Reflector sheet thickness, t	0.002 m
Reflectance of the mirror, ρ	0.840
The concentration ratio, C	11.70

The Receiver

The receiver is the most critical PTC component, directly affecting PTC performance. It was a black-painted red copper tube to enhance solar radiation absorbtance. It was enveloped by a borosilicate glass cylinder to prevent heat loss by convection, with a transmittance of 0.90 [38]. Specification of the receiver tube is given in Table 2. A representation of the receiver tube is demonstrated in Figure 5.

Table 2. Specification of the receiver tube.

Parameter	Value
Receiver absorptivity, α [39]	0.92
Copper tube length, L_c	1440 mm
Copper tube inside diameter, D_i	26.4 mm
Copper tube outside diameter, D_o	28.6 mm
Glass cover inside diameter, D_{gi}	54 mm
Glass cover outside diameter, D_{go}	60 mm
Glass tube length, L_g	1100 mm

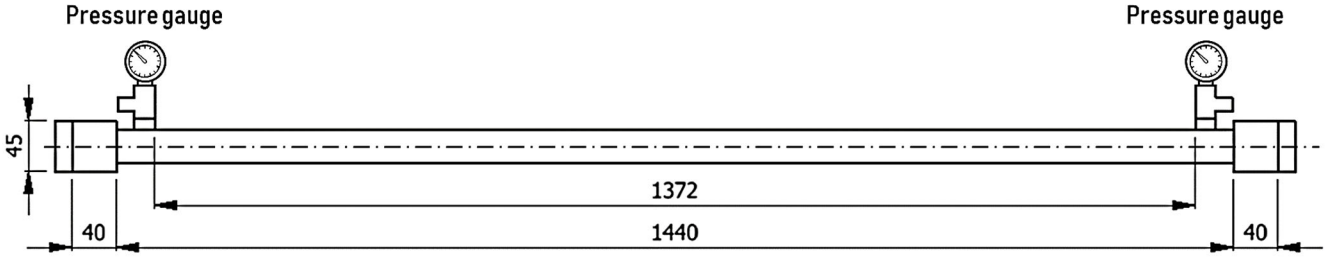

Figure 5. The receiver tube schematic diagram, dimensions in mm.

The Helical Shaft

Steel was selected as shaft material for its high strength, elasticity, and ability to withstand machining. Dimensions of the helical shaft are shown in Figure 6. The helical shaft was immersed in a nickel-chrome basin to prevent corrosion during experimental work. The two sides of the shaft were fixed onto an oil seal ring that bears a high temperature of 250 °C to prevent HTF leakage. Specification of the helical shaft is given in Table 3. DC motor gearbox of 24 V and 50 RPM was used to rotate the shaft at variable speeds of 4, 11, and 21 RPM, and it was connected to the shaft through a coupling and was fixed to the PTC structure.

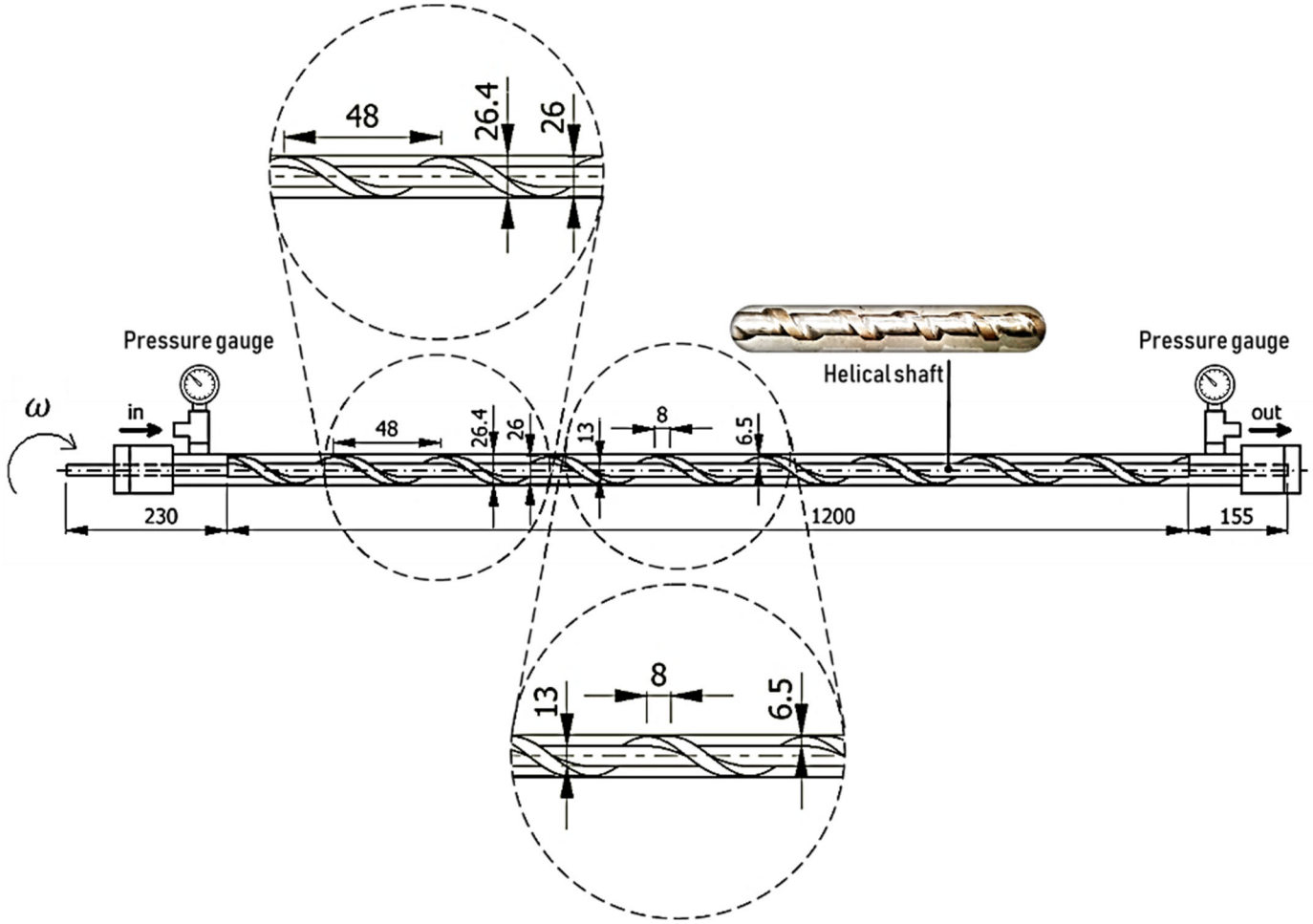

Figure 6. Longitudinal section of the helical shaft inside the receiver tube, dimensions in mm.

Table 3. Specification of the helical shaft.

Parameter	Value
The total length of the helical shaft, L_h	1585 mm
length of the helical section, l_h	1200 mm
Diameter of the helical shaft, D_h	26 mm
Pitch length of the helical shaft, p_h	48 mm
The thickness of the tooth, t_h	8 mm
Height of the tooth. H_h	6.5 mm

2.1.2. The Sun Tracking Mechanism

The PTC tracks the sun using a single-axis tracking approach where the tracking axis can be positioned in the East-West or the North-South directions. Since the North-South sun-tracking axis provides more solar energy yearly than the East-West sun-tracking axis [40], the collector was oriented to rotate about a horizontal North-South axis. The tracking mechanism consists of four light-dependent resistors (LDRs), detecting the solar irradiation and instructing the linear actuators through an Arduino circuit to track the sun.

2.1.3. The Measuring Instruments

The test rig was equipped with the following measuring instruments:

- Four K-type thermocouples with an accuracy of (±0.1 °C) were calibrated and employed to detect the HTF and ambient temperatures. Two were located at the receiver tube entrance and exit, one in the HTF tank and one in the ambient atmosphere.

- The average receiver surface temperature was determined by placing sixteen calibrated thermocouples on the copper tube's outer surface in circular and longitudinal directions, as illustrated in Figure 7. The thermocouples were connected to a data logger recording the measured values with a range of (−129–1372 °C).
- A digital portable solar power meter was used to measure the beam solar radiation at normal incidence through a scale of (1–1999 W/m^2) with an accuracy of (±10 W/m^2).
- A rotameter was employed to measure the volume flow rate with a scale of (0.5–4 LPM) and accuracy (±4% full scale) installed at the pump downstream.
- Since the HTF pressure is inversely proportional to the flow rate, three couples of pressure gauges were used to measure the pressure with an accuracy of (±1% full scale). Two pressure gauges were located at the receiver tube inlet and outlet to evaluate the pressure drop across the receiver under technical data and operating conditions listed in Table 4. The third couple of pressure gauge monitored the HTF pressure over the outdoor tests to maintain the HTF temperature below its saturation point to maintain the HTF in the liquid state.
- A digital multimeter (40 mA–10 A) was used to measure the DC motor power consumption with an accuracy of (±0.8% + 3).
- A digital tachometer measured the helical shaft rotating speed with a scale of (2–20,000 RPM) and accuracy (±0.05% + 1 digits).

Table 4. Specification of pressure gauges used and operating conditions.

Gauge Number	Range (Pa)	Resolution (Pa)	Range of Flow Rates (LPM) *
1	2500	50	0.5–1.0 (indoor tests)
2	16,000	100	1.5–2.5 (indoor tests)
3	250,000	10,000	0.5–2.5 (outdoor tests)

* The range of flow rates where the gauge is used to determine the pressure drop over the receiver.

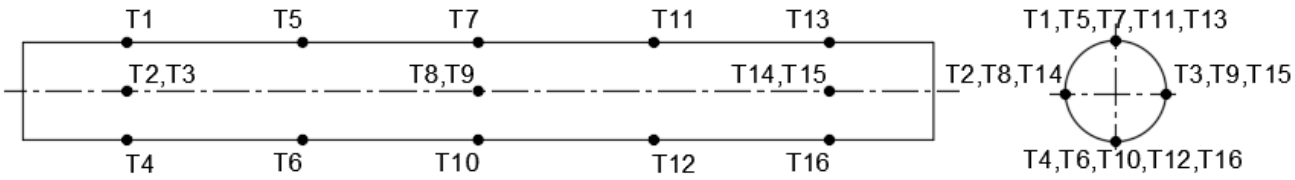

Figure 7. Thermocouple distribution over the copper tube surface.

2.1.4. System Operation

The outdoor experiments were conducted at Integrated Technical Education Institute, Cairo, Egypt. The latitude and the longitude of Cairo city are 30°02′ N and 31°14′ E, respectively. Using a linear actuator, the PTC axis was oriented to the North-South. The solar radiation HTF temperatures at the tank, ambient, test section inlet, and outlet were continuously detected and recorded. Over twenty-five clear days, within June, July, and August, the measured data were recorded every 15 min from 10:00 to 16:30. The irradiation over all experiments ranged from 600 to 1200 W/m^2. A 225 W pump circulated the HTF between the tank and the test section. After the HTF temperature increased in the receiver tube, the hot HTF was returned to the tank and then to the tube in a closed-loop cycle. The HTF flow rate was varied to obtain five variable flow rates of 0.5, 1, 1.5, 2, and 2.5 LPM using ball valves located at the inlet and exit of the HTF stream. DC motor rotational speeds (4, 11, and 21 RPM) were used.

2.2. Governing Equations

2.2.1. Friction Coefficient Evaluation

For Plain Receiver Tube

The average velocity (U_{av}) and Reynolds number (Re) are given as [6]:

$$U_{av} = \frac{\dot{V}}{\frac{\pi}{4} D_i{}^2} \tag{5}$$

$$\mathrm{Re} = \frac{U_{av}\ D_i}{v} \tag{6}$$

For the Receiver with Helical Shaft Insert

U_{av} and Re are determined based on the measured flow rate according to the equivalent hydraulic diameter, D_{eq}. Where D_{eq} is evaluated experimentally by measuring the HTF volume, V, required to fill the entire length of the copper tube, L_c with the helical shaft insert as follows [41]:

$$V = \pi/4\ D_{eq^2}\ \times\ L_c \tag{7}$$

$$D_{eq} = (4V/\pi L_c)^{0.5} \tag{8}$$

The Re number of the flow within a tube is estimated as follows [42]:

$$\mathrm{Re} = \frac{U_{av}\ D_{eq}}{v} \tag{9}$$

where v is the kinematic coefficient of viscosity of water and U_{av} is the average velocity in the receiver tube with helical shaft insert; determined from as:

$$U_{av} = \frac{\dot{V}}{\frac{\pi}{4} D_{eq}{}^2} + Np \tag{10}$$

where $\dot{V}$ is the volumetric flow rate of the HTF, N is the number of revolutions per minute, and p is the helical shaft pitch.

The Darcy–Weisbach friction factor is described as [18,30]:

$$f = \frac{\Delta P}{0.5\ \rho_f\ U_{av}{}^2\ \frac{l}{D_{eq}}} \tag{11}$$

where ΔP is pressure drop difference between pipe inlet and exit, that is determined experimentally, ρ_f is the density of HTF at the average bulk temperature $\left[T_{av} = 0.5(T_{fo} + T_{fi})\right]$ and l is the test section length (1.372 m).

2.2.2. Nusselt Number Evaluation

The average inner wall temperature of the receiver is [20,22]:

$$T_{wi}{}^{\sim} = T_{wo}{}^{\sim} - \frac{Q_u\ \ln\ (D_o/D_i)}{2\pi k_c l} \tag{12}$$

$$T_{wo}{}^{\sim} = \frac{\sum T_{wo}}{16} \tag{13}$$

where k_c, $T_{wo}{}^{\sim}$ are the thermal conductivity of the copper and average outer wall temperature of the receiver, respectively.

Log mean temperature difference:

$$LMTD = (\Delta T_1 - \Delta T_2)/ln\ (\Delta T_1/\Delta T_2) \tag{14}$$

where:

$$\Delta T_1 = T_{wi}{}^{\sim} - T_{fi} \tag{15}$$

$$\Delta T_2 = T_{wi}{}^{\sim} - T_{fo} \tag{16}$$

The average heat transfer coefficient for HTF was calculated by [43]:

$$h = \frac{Q_u}{A_i \, LMTD} \tag{17}$$

where Q_u is the heat absorbed by HTF. A_i is the inner surface area of the receiver, which can be expressed as:

$$A_i = \pi D_i l \tag{18}$$

The average Nusselt number is determined as follows [18]:

$$Nu = \frac{hD_{eq}}{k} \tag{19}$$

2.3. Performance Evaluation

2.3.1. Thermal Enhancement Factor

The thermal enhancement factor (TEF) is the ratio of the augmented surface heat transfer coefficient (inserted receiver tube), h, to that of a smooth surface (plain receiver tube), h_o, at the same pumping power. It is given as [11]:

$$TEF = \left[\frac{h}{h_o}\right]_{pp} = \left[\frac{Nu}{Nu_o}\right]_{pp} = \frac{(Nu/Nu_o)}{(f/f_o)^{(1/3)}} \tag{20}$$

where Nu and Nu_o are for the receiver with insert and the receiver without insert, respectively. The same is true for the friction factor (f and f_o).

2.3.2. Thermal Efficiency

The thermal efficiency is the heat absorbed by HTF (Q_u) to the total incident direct irradiance to the collector aperture. The instantaneous thermal efficiency can be determined as follows [36]:

$$\eta_{th,i} = \frac{Q_{u,i}}{H_{bn,i} \, A_a} \tag{21}$$

$$`Q_{u,i} = \dot{m}_f C_p \left(T_{fo} - T_{fi}\right)_i \tag{22}$$

The average daily thermal efficiency is:

$$\eta_{th} = \frac{Q_u}{Q_s} = \frac{\sum Q_{u,i}}{\sum H_{bn,i} A_a} \tag{23}$$

$$`Q_u = \sum Q_{u,i} \tag{24}$$

$$Q_s = \sum H_{bn,i} A_a \tag{25}$$

where i = 1, 2, . . . , n and n is the number of time intervals in the day.

T_{fi}, T_{fo}, H_{bn} and A_a are the inlet and outlet temperatures of the HTF, normal beam solar radiation at the collector plane, and aperture area, respectively.

2.3.3. Overall Efficiency

The average daily overall efficiency, η_{ov}, evaluates the net heat production, which can be represented as [44]:

$$\eta_{ov} = \frac{Q_u - \frac{P_p}{\eta_{el}} - P_{mo}}{Q_s} \tag{26}$$

where η_{el} and η_P are electrical and pump efficiency, 0.327 and 0.80, respectively [45–47]. While P_P and P_m are the pumping power and the power of the DC rotating motor, respectively. The pumping power is a critical parameter as using its value increases as a side effect of applying an insert turbulator within the thermal receiver. It can be calculated as follows [44]:

$$P_P = \frac{\Delta P\ V}{\eta_p} \tag{27}$$

2.3.4. Exergtic Efficiency

The exergtic efficiency of the PTC, η_{ex}, is a critical parameter that indicates the maximum work production extracted from the PTC, which is given below [48]:

$$\eta_{ex} = \frac{E_u}{E_s} \tag{28}$$

where, E_u and E_s are the useful output exergy of the HTF and the available solar exergy, respectively. E_u is obtained by [49]:

$$E_u = Q_u\left(1 - \frac{T_{am}}{T_m}\right) - \frac{T_{am}}{T_m}W_T \tag{29}$$

where, W_T is the total of power consumed by the pump and the DC motor. The power consumption of the DC motor is equal to 26.40, 13.68, and 7.44 at speeds of 4, 11, and 21 RPM, respectively. The available solar exergy is obtained from [50,51]:

$$E_s = Q_s\left(1 - \frac{4}{3}.\frac{T_{am}}{T_{sun}} + \frac{1}{3}.\left[\frac{T_{am}}{T_{sun}}\right]^4\right) \tag{30}$$

The mean temperature of fluid, T_m, can be written as [52]:

$$T_m = \frac{\left(T_{fo} - T_{fi}\right)}{ln\left(T_{fo}/T_{fi}\right)} \tag{31}$$

T_{am} is the ambient temperature and T_{sun} is the sun temperature, and it is equal to 5770 K.

The uncertainty analysis in experimental measuring parameters was presented by [53,54], which could be determined using a root–sum–square combination of each of the individual inputs. For example, the uncertainty of a function X can be determined as follows:

$$w_X = \sqrt{\left(\frac{\partial X}{\partial x_1}\ w_1\right)^2 + \left(\frac{\partial X}{\partial x_2}\ w_2\right)^2 + \cdots \left(\frac{\partial X}{\partial x_n}\ w_n\right)^2} \tag{32}$$

where w_X is the uncertainty of the value X, w is the uncertainty of the measured parameter, and X is a given function of the independent variables $x_1, x_2, x_3, \ldots, x_n$. Thus, $X = X(x_1, x_2, x_3, \ldots, x_n)$.

And then, the relative error λ_R is defined as:

$$\lambda_R = \frac{w_X}{X} \tag{33}$$

The relative error of friction factor, Nu number, thermal efficiency, and overall efficiency are 9.29%, 5.10%, 4.92%, and 5.12%, respectively.

3. Results and Discussion

The experimental runs were performed for three cases: (1) plain receiver tube (without insert), (2) receiver with stationary helical shaft (SHS) insert, and (3) receiver with helical shaft (RHS) insert rotating with different rotational speeds of 4 RPM (RHS1), 11 RPM

(RHS2), and 21 RPM (RHS3). All cases were tested at HTF flow rates of 0.5, 1.0, 1.5, 2.0, and 2.5 LPM. The data were continuously recorded every 15 min. A nomenclature summary of the tested cases is listed in Table 5.

Table 5. Nomenclature of tested cases; denotations and conditions.

Case	Denotation	Insert Rotating Speed (RPM)
WIR	Without-insert receiver (Plain tube)	–
SHS	Stationary helical shaft receiver	0
RHS1	Rotating helical shaft receiver—Case 1	4
RHS2	Rotating helical shaft receiver—Case 2	11
RHS3	Rotating helical shaft receiver—Case 3	21

All cases are tested at HTF flow rates of 0.5, 1.0, 1.5, 2.0, and 2.5 LPM.

The variation of Re with flow rate is presented in Figure 8. It can be noted that the Re rises with increasing the flow rate for all cases due to the axial velocity increase with the flow rate, while at the same flow rate, the axial velocity increased in the RHS cases more than in the SHS case as the axial velocity increased with the helical shaft rotation.

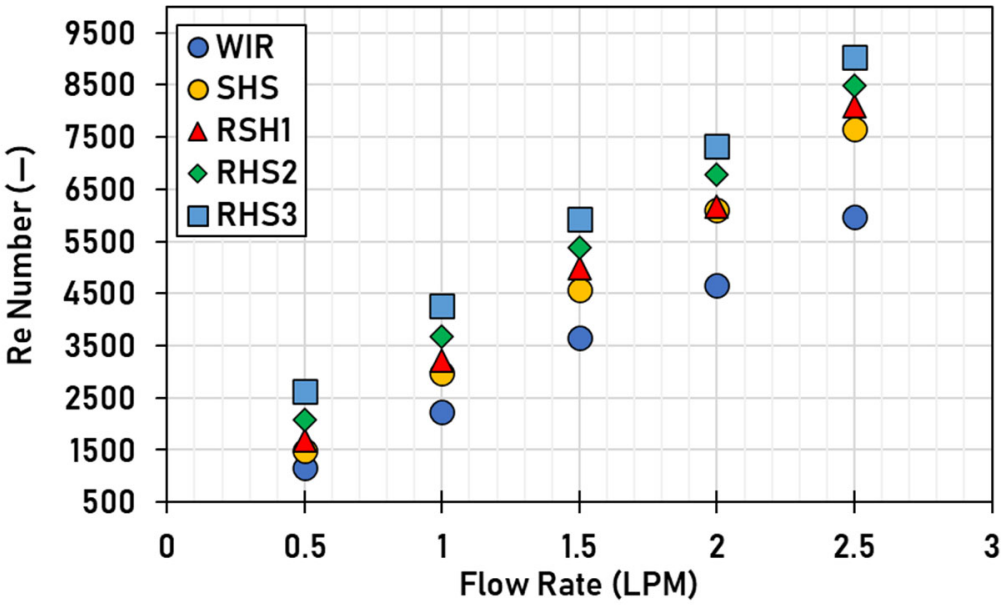

Figure 8. Reynolds number against flow rate in all tested cases.

Figure 9 shows the average heat transfer coefficient for all the examined cases of the PTC, which clearly shows that increasing the value of the average heat transfer coefficient with increasing the flow rate, which may be explained because more flow disturbance is created along the tube walls when the flow rate increases. Intense swirls enhance the fluid mixing between the core and near the wall regions and consequently enhance the average heat transfer coefficient by increasing the flow rate. In the cases of SHS and RHS and at a constant HTF flow rate, the helical shaft increases the intensity of swirl flow and resulting in higher contact surface area between the receiver and HTF, leading to an increase in the useful heat gain and consequently enhancing the average heat transfer coefficient with introducing SHS and RHS.

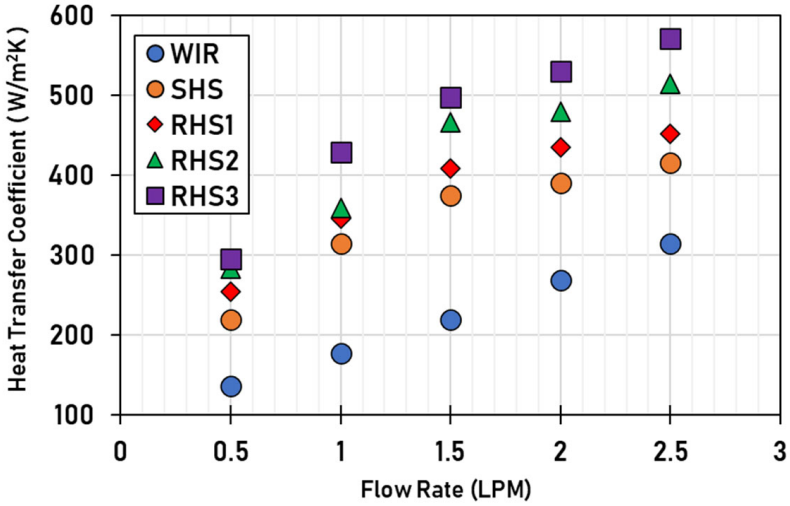

Figure 9. Average heat transfer coefficient against flow rate.

The variation of the Nu number corresponding to the average heat transfer coefficient in Figure 9 is shown in Figure 10a. The Nu number ratio with flow rate variation is illustrated in Figure 10b. The higher Nu number ratio is achieved at 1 LPM compared to the other flow rates, and it achieves a maximum of 2.42 for the case of RSHS3. Furthermore, the Nu number ratio decreases with the rise of flow rate from 1.5 LPM to 2.5 LPM for all cases, while at 0.5 LPM, the Nu number ratio reaches a higher value of 2.17 for the case of RSHS3 and reaches a lower value of 1.62 for the case of SHS.

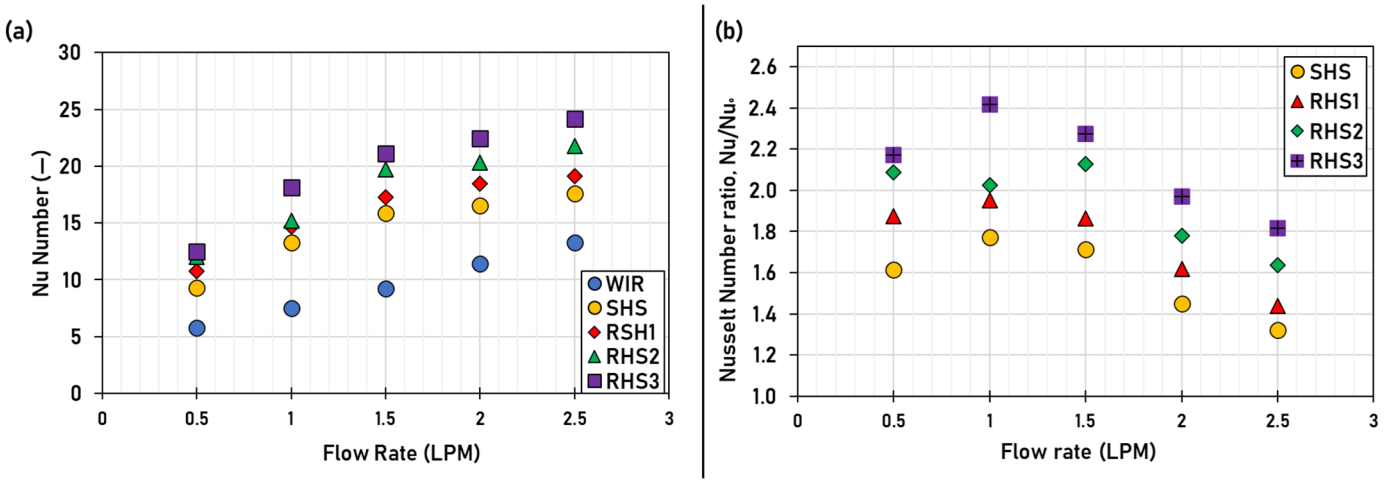

Figure 10. Nusselt number relations ratio against flow rate. (**a**) Nusselt number against flow rate. (**b**) Nusselt number ratio against flow rate.

The thermal efficiencies of all tested cases are shown in Figure 11. It can be noted that the instantaneous thermal efficiency varies with the experiment time over the day due to the rapid incident solar radiation variation. However, the thermal efficiency slightly varies when inserted the helical shaft inside the receiver tube since the helical shaft can compensate for the incident solar radiation variations over the daytime. Moreover, Figure 11a to Figure 11e indicate that increasing the helical shaft insert's rotation speed results in higher and more stabilized instantaneous thermal efficiency over the daytime. This result may be attributed to improved mixing, more intense secondary flow, and higher thermal boundary layer disruption due to shaft rotation. As a consequence, the convective heat transfer is improved.

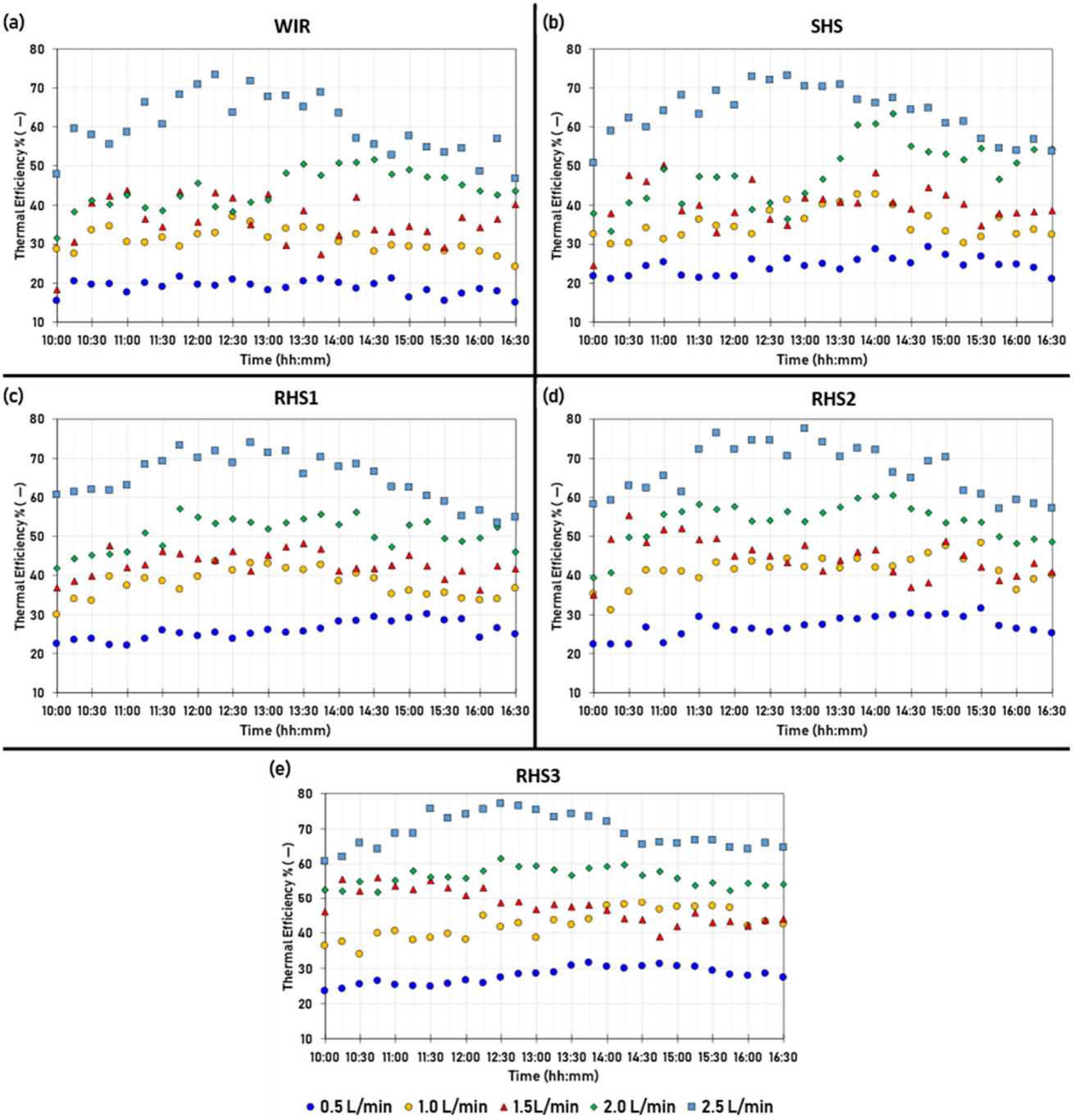

Figure 11. The instantaneous thermal efficiency against time in all tested cases.

Figure 12 shows temperature differences at a different flow rate for all cases. As the flow rate decreases from 2.5 to 0.5 LPM, the temperature difference increases, as stated in [55]. The reason is that, at the low flow rate, the HTF has a long time to increase its temperature along the receiver tube, so the temperature difference has a higher value. On the contrary, the HTF does not have enough time to increase its temperature at a high flow rate, so the temperature difference has a lower value.

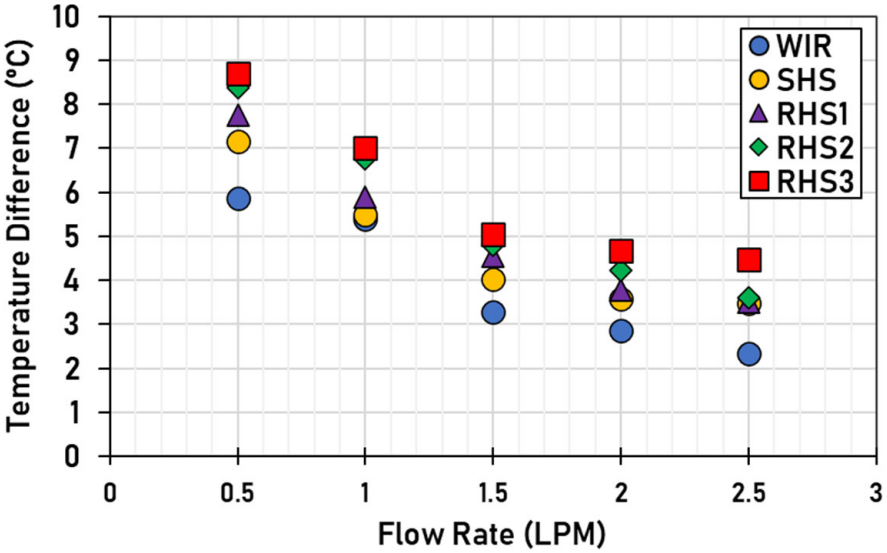

Figure 12. Temperature difference against flow rate.

Compared to a plain tube, the temperature differential is enhanced by using an insert within the receiver at a constant HTF flow rate. Furthermore, due to expanding the contact surface area for HTF with the shaft, the convective heat transfer rate is enhanced, and higher outlet temperature is observed, consequently increasing temperature difference. In addition, when the helical shaft rotates, it causes more intense secondary flow, more disturbance of the thermal boundary layer, and improved mixing. Consequently, the convective heat transfer rate and outlet temperature increase the temperature difference.

In addition, from Figure 13a, it can be observed that the increase in the HTF flow rate boosts the instantaneous thermal efficiency. These observed results are not limited to the instant thermal efficiency. However, they extend to average daily thermal efficiencies, as illustrated in Figure 13a. The thermal efficiency increase with increasing the flow rate is compatible with what was stated in [52,56] due to higher confrontation between the HTF particles and higher turbulence and, as a result, augmented thermal performance and efficiency. In the cases of RHS1, RHS2, and RHS3, the rotating helical shaft amplifies the intensity of swirl flow and enhances thermal efficiency compared to SHS. The efficiency of PTC for WIR, SHS, RHS1, RHS2, and RHS3 varies from 19% to 60.3%, 24.51% to 63.82%, 25.9% to 65.02%, 27.1% to 66.9%, and 27.9% to 69.25% with flow rate ranging from 0.5 to 2.5 LPM.

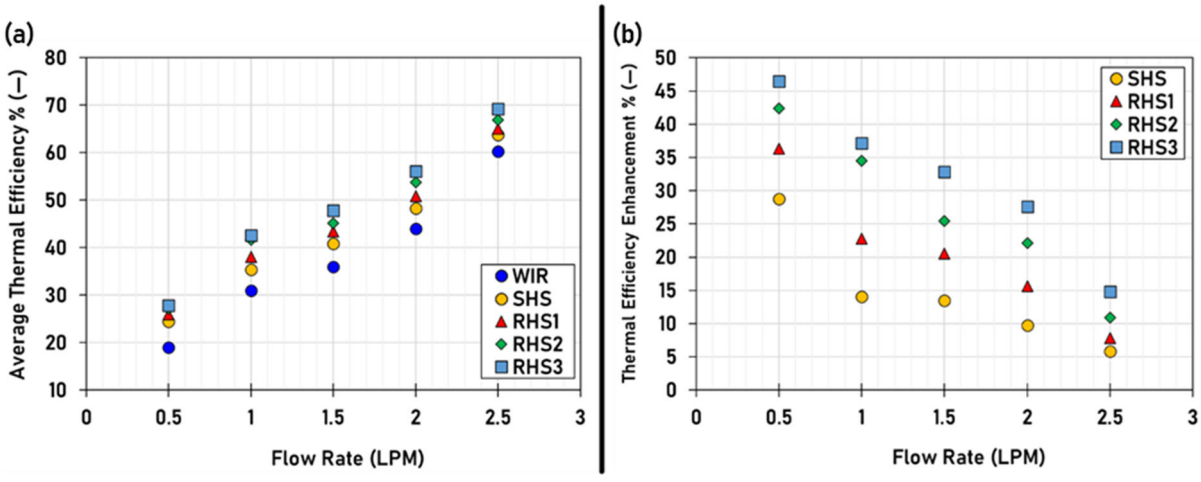

Figure 13. Thermal efficiency against flow rate. (**a**) Average daily efficiency vs. flow rate. (**b**) Efficiency enhancement % vs. flow rate.

However, the thermal efficiency enhancement, as plotted in Figure 13b, is observed to decrease with the rise of flow rate as the rate of growth of thermal efficiency for the plain tube with increasing flow rates is higher than the rate of growth in thermal efficiency for the receiver tube fitted with stationary or rotating helical shaft. As a result, the enhancement in thermal efficiency is reduced with increasing flow rates. Moreover, the enhancement is higher when the shaft rotates at a higher rotational speed than the stationary one. Using RHS3 leads to the maximum enhancement, ranging from 14.82 to 46.47% while using SHS leads to enhancement from 5.82% up to 28.78% compared to the plain tube.

The friction factor against flow rates for all tested cases is evaluated and plotted as illustrated in Figure 14a. As noted, the friction factor reduces as the flow rate increases, as indicated in [52]. Moreover, it increases in the cases of SHS, RHS1, RHS2, and RHS3 compared to the plain tube. This is because the shaft causes increases in swirl flow intensity, residence time, and contact surface area for SHS. In contrast, the long time inside the receiver tube increases the contact between the HTF particles and the receiver tube wall and, as a result, increases the friction factor and pressure drop. Moreover, for the cases of RHS1, RHS2, and RHS3, increasing the rotational speed magnifies the intensity of swirl flow and turbulence. As a result, it makes the HTF move over the longer paths, increasing the friction factor compared to RSHS. Consequently, the maximum friction factor is 1.3, and it is reached at a lower flow rate of 0.5 LPM and a higher rotational speed of 21RPM (RHS3), while the lower friction factor is 0.156 and reached at a higher flow rate of 2.5 LPM and stationary insert (SHS). Therefore, the friction factor ratio reduces with the growth in flow rate, while for the RHS3 and SHS cases, the friction factor ranges from 4.1 to 7.7 times and 1.9 to 4.1 times, respectively, compared to the WIR case, as seen in Figure 14b.

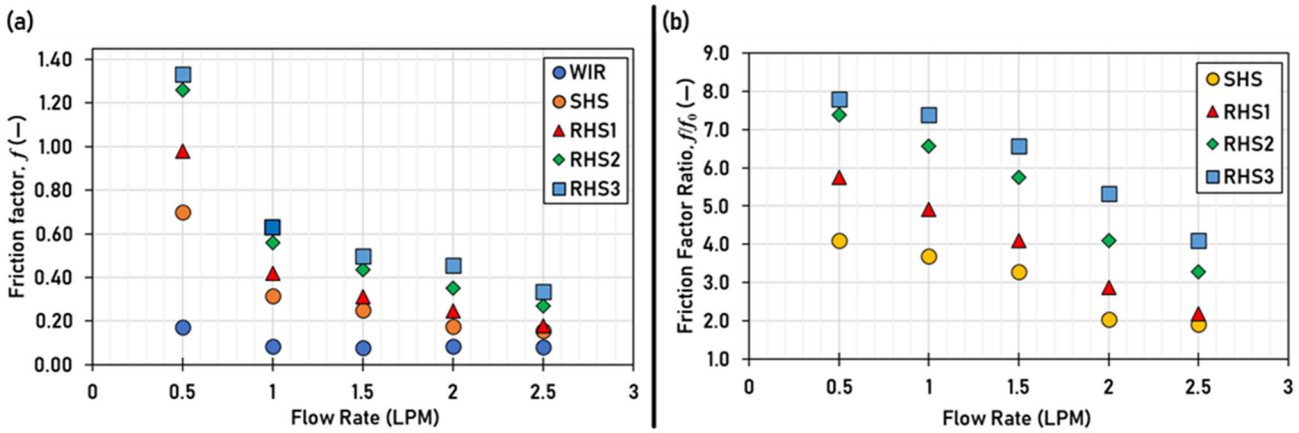

Figure 14. Friction factor against flow rate. (**a**) Friction factor vs. flow rate. (**b**) Friction factor ratio vs. flow rate.

The pumping power increases by increasing the flow and using the helical shaft insert, as illustrated in Figure 15a and stated in [18]. Moreover, using a shaft insert leads to higher pumping power in the cases of SHS, RHS1, RHS2, and RHS3 compared with the WIR. Raising the flow rate from 0.5 to 2.5 LPM increases the pressure drop from 250 to 1400 Pa, 350 to 1600 Pa, 450 to 2400 Pa, and 500 to 3000 Pa in the cases of SHS, RHS1, RHS2, and RHS3, respectively, and consequently increasing pumping power. However, the increase in pumping power, as plotted in Figure 15b, is observed to reduce with the flow rate rise as the pumping power is greater for the plain tube when increasing the flow rates compared to the rate of growth in pumping power for the receiver tube fitted with stationary or rotating helical shaft. As a result, the percentage rise in pumping power is decreased with rising flow rates. Moreover, the increase is higher when the shaft rotates at a higher rotational speed than the stationary one. Using RHS3 leads to the maximum increase, ranging from 404 to 850%, while using SHS increases 130 to 400% compared to the plain tube.

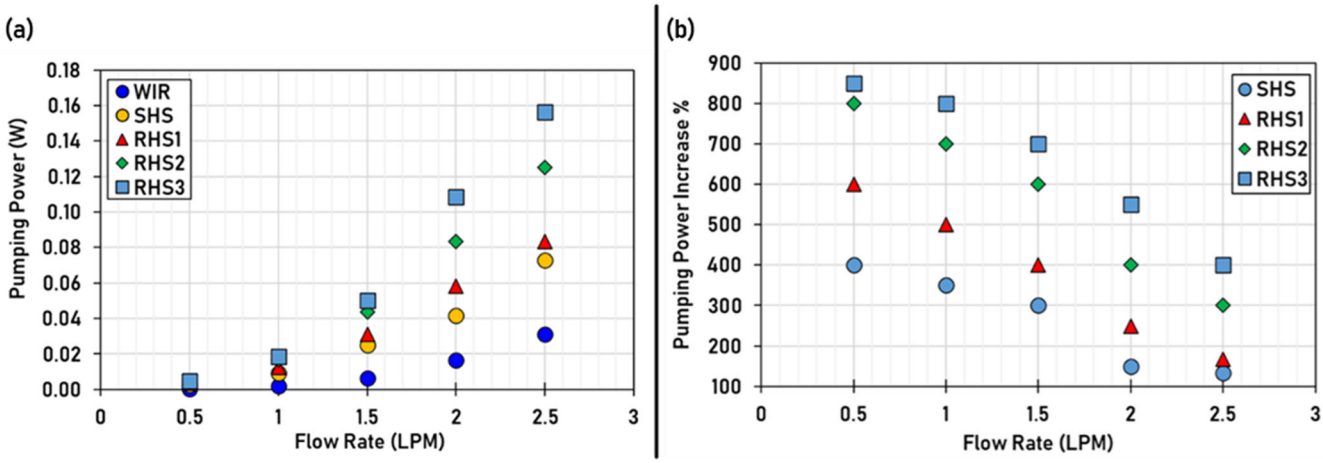

Figure 15. Pumping power relations ratio against flow rate. (**a**) Pumping power against flow rate (**b**) % increase in pumping power against flow rate.

Considering the effect of power consumed in the pump and the DC motor rotating the helical shaft, the overall efficiency can be used to evaluate the system; as shown in Figure 16a. It indicates an improvement of thermal efficiency for all cases with the flow rate increase due to the slight rise in the total power consumed compared to the higher growth in beneficial heat gain. So, the overall efficiency trend is the same for thermal, and the overall efficiencies enhancement is the same for the thermal efficiency enhancement, as shown in Figure 16b.

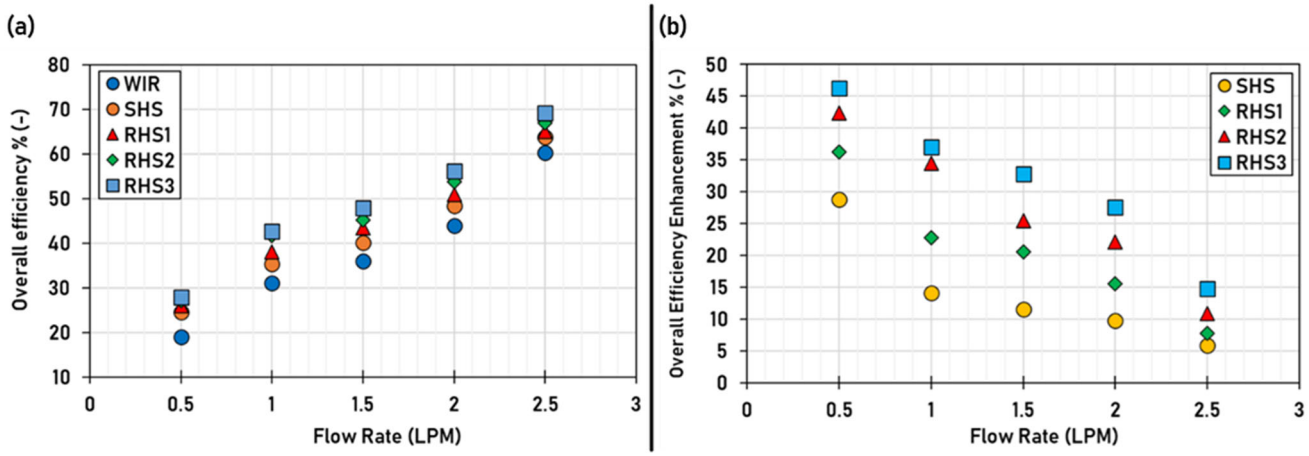

Figure 16. Efficiency relations against flow rate. (**a**) Overall efficiency against flow rate. (**b**) % enhancement of overall efficiency.

Figure 17 shows the variations of TEF against flow rate. TEF for all cases is higher than unity, while the heat transfer enhancement is higher than the pressure drop rise. The maximum TEF is 1.24, achieved at 1 LPM and in the case of RHS3.

The exergy efficiency with various flow rates in all tested cases is shown in Figure 18. Based on results plotted in Figure 18, raising the flow rate from 0.5 to 2.5 LPM increases the useful heat gain and results in exergy efficiency enhancement from 11.11% to 36.35% in the plain tube case stated in [50]. Inserting the helical shaft increases exergy efficiency from 14.16, 14.52, 15.14, and 15.23% to 37.81, 39.21, 38.98, and 40.41% for the cases of SHS, RHS1, RHS2, and RHS3, respectively, with raising the flow rate from 0.5 to 2.5 LPM. This result is attributed to the rising logarithmic mean temperature of the fluid, T_m. With boosting the flow rate that leads to both decreasing in the second term ($T_0/T_m W_T$) and increasing the useful heat gain in the first term and consequently increasing the exergy

efficiency. Increasing the total power consumption at the same flow rate due to rotating the helical shaft in the cases of RHS1, RHS2, and RHS3 does not prevent enhancing the exergy efficiency because the rate of increasing the useful heat gain is higher than increasing the total power consumption that leads to enhancement in exergy efficiency.

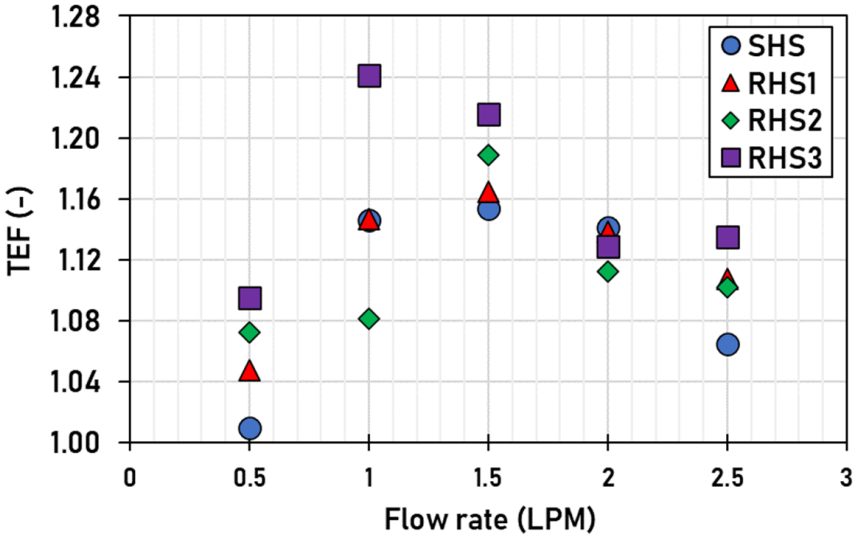

Figure 17. Variation of TEF against flow rate.

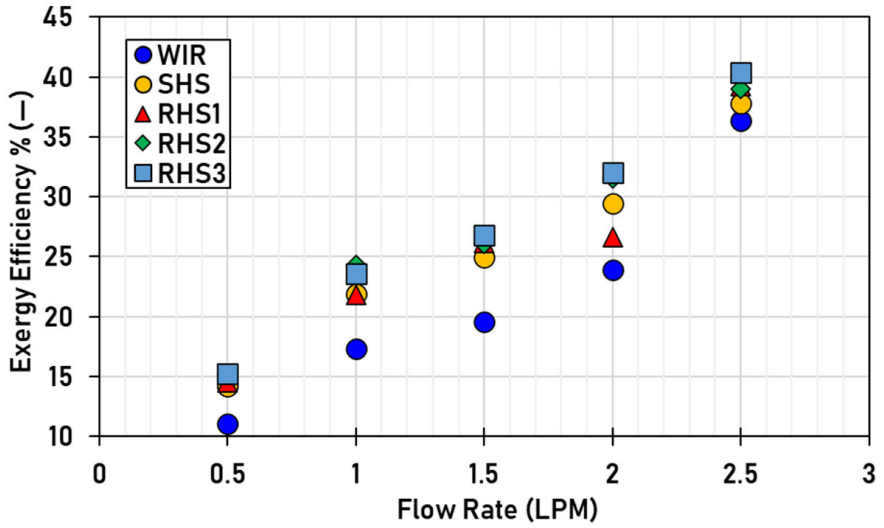

Figure 18. Exergetic efficiency against flow rate.

A comparison between the present work (static and rotating helical shaft) and different types of inserts in terms of thermal efficiency ratio, Nu number ratio, and friction ratio is provided in Table 6. The highest efficiency ratio is 2.33 for wire matrix and twisted tape [29]. On the other hand, they achieved a higher friction ratio of 36.02.

The filling porous [57] achieved a maximum Nu number ratio of 17.24 and a maximum friction factor ratio of 412.62. According to the reviewed literature, using twisted tape and fins can lead to higher thermal enhancement with a lower impact on the friction factor. The experimental study of the static helical shaft has a higher efficiency ratio of 1.28 and a lower friction ratio of 4.10 compared with a numerical study of twisted tape of 1.07 and a higher friction factor ratio of 6.15. While using the rotating helical shaft in the current study led to a maximum efficiency ratio of 1.46 and a maximum Nu number ratio of 2.41 compared to fins and twisted tape, but as a penalty of maximum friction factor ratio of 7.79.

Table 6. Comparison between present work and various inserts inside PTC.

Study Type	Type of Insert	η/η_o	Nu/Nu_o	f/f_o	Ref.
Exp.	Copper foam	1.03–1.08	1.01–1.80	95–250	[32]
Exp.	Wire matrix and twisted tape	1.35–2.33	1.67–2.60	36.02	[29]
Num.	Toroidal rings	1.00–1.037	1.00–2.33	1.00–14.62	[58]
Num.	Perforated plate	1.005–1.018	1.8–2.0	13.34–13.46	[59]
Num.	Filling porous	1.07	3.49–17.24	17.60–412.62	[57]
Num.	Twisted tape	1.005–1.015	1.70–1.77	4.17–6.15	[59]
Num.	Internal longitudinal fins	1.37–1.41	1.96–2.19	2.03–2.12	[60]
Exp.	Static helical shaft	1.05–1.28	1.32–1.77	1.91–4.10	Present work
Exp.	Rotating helical shaft	1.06–1.46	1.43–2.41	2.18–7.79	Present work

4. Economic Analysis

The utility of using the inserts inside PTC can be evaluated based on its economic viability. Fixed cost (FC) and annual variable cost (VC) are considered in order to estimate the total cost of PTC, while the initial cost is estimated by considering all components of building a system, and the operating cost is estimated by considering the effect of power consumed in the pump and DC motor. The cost data of components of PTC for three WIR, SHS, and RHS cases are listed in Table 7 according to the Egyptian market. The economic analysis is carried out at maximum TEF, achieved at 1 LPM and RHS3.

Table 7. The cost data of various components of PTC.

Sr.	Details of Component	Quantity (Units)	Unit Cost (USD/Unit)	Total Cost (USD)
1	Acrylic reflector sheet	1	66.7	66.7
2	Copper tube	1	16.7	16.7
3	Glass tube	1	11.1	11.1
4	Linear actuator	1	17.8	17.8
5	Pipes and accessories	1	31.4	31.4
6	valves	5	2.2	11.1
7	Storage water tank	1	38.9	38.9
8	Silicon	5	0.8	4.2
9	Insulation material	1	16.7	16.7
10	Circulation pump	1	19.4	19.4
11	ARDUINO circuit	1	33.3	33.3
12	Batteries	2	38.9	77.8
13	The metallic structure of PTC	1	61.1	61.1
14	Manufacture cost	1	55.6	55.6
A	**Total fixed cost**		**WIR**	**462**
15	Insert tape (steel)	1	27.8	27.8
16	Manufacture cost	1	61.1	61.1
B	**Total fixed cost**		**SHS**	**551**
17	Oil seal ring	2	2.2	4.4
18	DC motor gearbox and control circuit	1	25.0	25.0
19	Coupling	1	2.5	2.5
C	**Total fixed cost**		**RHS**	**583**

Bold rows (A, B, and C) represent the summation of total fixed costs of each case (WIR, SHS, and RHS), respectively.

Total Cost Estimation of PTC

The annual cost of useful heat per kWh (ACUH) can be calculated as follows [54]:

$$ACUH = TC/TUH \quad (34)$$

where, TC is the total cost and can be determined from Equation (35), while TUH is the total useful heat during the life span and is expressed by Equation (36).

$$\text{TC} = \text{FC} + \text{VC} \tag{35}$$

$$\text{TUH} = n \times \text{Yearly productivity} \tag{36}$$

where, n is the expected PTC lifetime, assumed to be 10 years. The yearly productivity can be calculated as follows:

$$\text{Yearly productivity} = (Q_u/\text{day}) \times \text{operating days} \tag{37}$$

where, the operating days were assumed to be 340 sunny days per year and (Q_u/day) is the useful heat per day for one cycle can be calculated as follows:

$$(Q_u/\text{day}) = Q_u \times \text{operating hours} \tag{38}$$

where, the operating hours were 7 h (from 9:30 to 16:30).

The economics of different cases of PTC based on estimated ACUH are presented in Table 8.

Table 8. The economic analysis for PTC with WIR, SHS, and RHS.

	WIR	**SHS**	**RHS**
Fixed cost (FC), USD	462	551	583
Annual variable cost (VC), USD	0.0004	0.0014	5.810
(Q_u/day), kWh	2.5	2.8	3.4
TUH, kWh	8414.3	9405.8	11,543.0
Total cost (TC), USD	462	551	588.4
ACUH, USD	0.055	0.059	0.051

The economic analysis in Table 8 shows that ACUH for PTC with WIR, SHS, and RHS are USD 0.055, USD 0.059, and USD 0.051, respectively. PTC with RHS has minimum ACUH, while SHS with PTC uses maximum ACUH. Therefore, using RHS is beneficial from an economic point of view compared to WIR and SHS, and using SHS without rotation has a poor impact on ACUH.

5. Conclusions

The influence of inserting a stationary and rotating helical shaft within the receiver on PTC performance was investigated in the present study. Three cases were investigated: A PTC without helical shaft insert, a PTC with stationary helical shaft insert, and a PTC with rotating helical shaft insert. The experiments were performed for different shaft rotational speeds of (4, 11, and 21 RPM) and various flow rates (0.5, 1, 1.5, 2, and 2.5 LPM) of water as an HTF. Moreover, the fluid flow and thermal parameters (friction factor, Re number, Nu number, and TEF) and performance parameters (thermal, overall, and exergetic efficiencies) were investigated. The following are the key findings of this investigation:

- The helical shaft insert has increased the required pumping power for the same flow rate.
- The pumping power rises with the shaft rotating speed, particularly at the high HTF flow rate.
- For the same flow rate, the helical shaft insert has enhanced the thermal performance (thermal, overall, and exergetic efficiencies) of the PTC.
- The thermal performance enhancement increases with growing the shaft rotating speed and the HTF flow rate.
- Compared to WIR, the friction factor ratios for RHS3 are higher than SHS, which are in the ranges of 4.1 to 7.79 times and 1.91 to 4.10 times, respectively. Furthermore,

Nu number ratios for RHS3 are higher than SHS in the ranges of 1.81 to 2.41 and 1.32 to 1.77.

- The maximum enhancement in thermal efficiency is 46.47%, achieved at a minimum flow rate of 0.5 LPM and RHS3.
- The maximum exergy efficiency is 40.41%, achieved at a higher flow rate of 2.5 LPM and RHS3.
- A comparison between the investigated three cases at the same pumping power using criteria of TEF shows that the maximum enhancement in thermal performance occurs at an HTF flow rate of 1 LPM, and the percentage enhancement in thermal efficiency is about 37% at shaft rotational speed of 21 RPM.
- The cost analysis shows that ACUH for RHS (USD 0.051) is lower than WIR and SHS (USD 0.059) at maximum TEF.

It can be concluded that using static and rotating helical shaft insert inside the receiver of PTC may be used for solar heating processes and power generation applications to enhance the performance of the PTC with a low penalty on pumping power compared to the other inserts. In the future, the use of nanofluids or hybrid nanofluids with rotating helical shafts is recommended, in order to investigate their effects on the thermal and hydraulic performance of PTC. Furthermore, a PV system coupled with PTC to supply the DC motor with power should be planned to reduce power consumption.

Author Contributions: Conceptualization, M.T., M.B. and E.E.-N.; methodology, M.A. and M.T.; data analysis, M.A. and M.T.; investigation, M.A., M.T., M.B. and E.E.-N.; writing—original draft preparation, M.A.; writing—review and editing, M.A. and M.T.; visualization, M.T.; supervision, M.T., M.B. and E.E.-N. All authors have read and agreed to the published version of the manuscript.

Funding: The Article Processing Charge (APC) was funded by Mansoura University, Egypt.

Informed Consent Statement: Not applicable.

Acknowledgments: The publication fees of this article have been supported by Mansoura University.

Conflicts of Interest: The authors declare no conflict of interest.

Nomenclature

Symbols

C	concentration ratio (-)
C_p	specific heat capacity (J/kg K)
D	diameter (m)
E	exergy rate (W)
F	focal length (m)
f	friction factor (-)
H_{bn}	normal beam solar radiation (W/m^2)
H	height (m)
h	heat transfer coefficient, W/m^{2}K
L	copper tube length (m)
l	test section length (m)
$\dot{m}$	mass flow rate (kg/s)
N	revolutions per minute (RPM)
P	power (W)
p	pitch (m)
Q	heat rate (W)
S	reflector width (m)
T	temperature (°C)
t	thickness (m)
U	velocity (m/s)
V	volume (m^3)
$\dot{V}$	volumetric flow rate (m^3/s)
W	aperture width (m)

Subscripts

a	aperture
av	average
am	ambient
c	copper tube
el	electrical
eq	equivilant
ex	exergetic
f	fluid
g	glass tube
h	helical shaft
i	inner or inlet
m	logarithmic mean
mo	motor
o	outer or outlet
ov	overall
p	pump
PP	constant pumping power
s	solar
T	total
u	useful
w	wall

Abbreviations

HTF	heat transfer fluid

w	uncertainty (-)
Greek Letters	
α	absorptance (-)
γ	intercept factor (-)
Δ	difference (-)
η	efficiency (-)
λ	relative error (-)
μ	dynamic viscosity (kg/m.s)
v	kinematic coefficient of viscosity (m^2/s)
ρ_f	density of HTF (kg/m^3)
ρ	reflectance (-)
τ	transmittance (-)
ϕ	rim angle (°)
ω	angular velocity (rad/s)
LMTD	Log mean temperature difference
LPM	liter per minute
PTC	parabolic trough collector
RHS	rotating helical shaft receiver
SHS	stationary helical shaft receiver
TEF	thermal enhancement factor
WIR	without-insert receiver
ACUH	annual cost of useful heat per kWh
TC	total cost
TUH	total useful heat during the life span
FC	fixed cost
VC	annual variable cost
Dimensionless Numbers	
Nu	Nusselt number
Re	Reynolds number

References

1. Bilal, A.; Khan, M.N.; Zubair, M.; Bellos, E. Commercial Parabolic Trough CSP Plants: Research Trends and Technological Advancements. *Sol. Energy* **2020**, *211*, 1422–1458. [CrossRef]
2. Sarbu, I.; Sebarchievici, C. Introduction. In *Solar Heating and Cooling Systems*; Elsevier: Cambridge, MA, USA, 2017; pp. 1–11. ISBN 9780128116623.
3. Shouman, E.R.; Khattab, N.M. Future Economic of Concentrating Solar Power (CSP) for Electricity Generation in Egypt. *Renew. Sustain. Energy Rev.* **2015**, *41*, 1119–1127. [CrossRef]
4. Tawfik, M. A Review of Directly Irradiated Solid Particle Receivers: Technologies and Influencing Parameters. *Renew. Sustain. Energy Rev.* **2022**, *167*, 112682. [CrossRef]
5. Fernández-García, A.; Zarza, E.; Valenzuela, L.; Pérez, M. Parabolic-Trough Solar Collectors and Their Applications. *Renew. Sustain. Energy Rev.* **2010**, *14*, 1695–1721. [CrossRef]
6. Anabela, E.; Panduro, C.; Finotti, F.; Largiller, G.; Yngve, K. A Review of the Use of Nanofluids as Heat-Transfer Fluids in Parabolic-Trough Collectors. *Appl. Therm. Eng.* **2022**, *211*, 118346. [CrossRef]
7. Abed, N.; Afgan, I. An Extensive Review of Various Technologies for Enhancing the Thermal and Optical Performances of Parabolic Trough Collectors. *Int. J. Energy Res.* **2020**, *44*, 5117–5164. [CrossRef]
8. Kreith, F.; Goswami, D.Y. *Handbook of Energy Efficiency and Renewable Energy*; Taylor & Francis Group: New York, NY, USA, 2007.
9. Peng, H.; Li, M.; Liang, X. Thermal-Hydraulic and Thermodynamic Performance of Parabolic Trough Solar Receiver Partially Filled with Gradient Metal Foam. *Energy* **2020**, *211*, 119046. [CrossRef]
10. Parlamıs, H.; Ozden, E.; Sami, M. Experimental Performance Analysis of a Parabolic Trough Solar Air Collector with Helical-Screw Tape Insert: A Comparative Study. *Sustain. Energy Technol. Assess.* **2021**, *47*, 101562. [CrossRef]
11. Sharma, M.; Jilte, R. A Review on Passive Methods for Thermal Performance Enhancement in Parabolic Trough Solar Collectors. *Int. J. Energy Res.* **2021**, *45*, 4932–4966. [CrossRef]
12. Kumar, C.N.; Murugesan, P. Review on Twisted Tapes Heat Transfer Enhancement. *Int. J. Sci. Eng. Res.* **2012**, *3*, 1–9.
13. Mousa, M.H.; Miljkovic, N.; Nawaz, K. Review of Heat Transfer Enhancement Techniques for Single Phase Flows. *Renew. Sustain. Energy Rev.* **2021**, *137*, 110566. [CrossRef]
14. Hasanpour, A.; Farhadi, M.; Sedighi, K. A Review Study on Twisted Tape Inserts on Turbulent Flow Heat Exchangers: The Overall Enhancement Ratio Criteria. *Int. Commun. Heat Mass Transf.* **2014**, *55*, 53–56. [CrossRef]
15. Allam, M.; Tawfik, M.; Bekheit, M.; El-Negiry, E. Heat Transfer Enhancement in Parabolic Trough Receivers Using Inserts: A Review. *Sustain. Energy Technol. Assess.* **2021**, *48*, 101671. [CrossRef]
16. Garg, M.O.; Nautiyal, H.; Khurana, S.; Shukla, M.K. Heat Transfer Augmentation Using Twisted Tape Inserts: A Review. *Renew. Sustain. Energy Rev.* **2016**, *63*, 193–225. [CrossRef]
17. Waghole, D.R.; Warkhedkar, R.M.; Kulkarni, V.S.; Shrivastva, R.K. Experimental Investigations on Heat Transfer and Friction Factor of Silver Nanofliud in Absorber/Receiver of Parabolic Trough Collector with Twisted Tape Inserts. *Energy Procedia* **2014**, *45*, 558–567. [CrossRef]
18. Chaurasia, S.R.; Sarviya, R. Numerical and Experimental Thermal Performance with Entropy Generation Analysis on Tube with Helical Screw Tape Inserts at Number of Strips in Turbulent Flow. *Proc. Inst. Mech. Eng. Part C J. Mech. Eng. Sci.* **2021**, *235*, 1057–1070. [CrossRef]
19. Nakhchi, M.E.; Hatami, M.; Rahmati, M. Experimental Investigation of Heat Transfer Enhancement of a Heat Exchanger Tube Equipped with Double-Cut Twisted Tapes. *Appl. Therm. Eng.* **2020**, *180*, 115863. [CrossRef]
20. Arunachala, U.C. Experimental Study with Analytical Validation of Energy Parameters in Parabolic Trough Collector with Twisted Tape Insert. *J. Sol. Energy Eng.* **2020**, *142*, 1–12. [CrossRef]

21. Hosseinalipour, S.M.; Rostami, A.; Shahriari, G. Numerical Study of Circumferential Temperature Difference Reduction at the Absorber Tube of Parabolic Trough Direct Steam Generation Collector by Inserting a Twisted Tape in Superheated Region. *Case Stud. Therm. Eng.* **2020**, *21*, 100720. [CrossRef]
22. Elton, D.N.; Arunachala, U.C. Twisted Tape Based Heat Transfer Enhancement in Parabolic Trough Concentrator—An Experimental Study. *IOP Conf. Ser. Mater. Sci. Eng.* **2018**, *376*, 012034. [CrossRef]
23. Ghadirijafarbeigloo, S.; Zamzamian, A.H.; Yaghoubi, M. 3-D Numerical Simulation of Heat Transfer and Turbulent Flow in a Receiver Tube of Solar Parabolic Trough Concentrator with Louvered Twisted-Tape Inserts. *Energy Procedia* **2014**, *49*, 373–380. [CrossRef]
24. Song, X.; Dong, G.; Gao, F.; Diao, X.; Zheng, L.; Zhou, F. A Numerical Study of Parabolic Trough Receiver with Nonuniform Heat Flux and Helical Screw-Tape Inserts. *Energy* **2014**, *77*, 771–782. [CrossRef]
25. Mohammed, A.A.; Mohammed, A.A.; Falleh, M.A. Heat Transfer Augmentation in Tube Fitted with Rotating Twisted Tape Insert. *J. Mech. Eng. Res. Dev.* **2020**, *43*, 308–316.
26. Qi, C.; Wang, G.; Yan, Y.; Mei, S.; Luo, T. Effect of Rotating Twisted Tape on Thermo Hydraulic Performances of Nano Fluids in Heat Exchanger Systems. *Energy Convers. Manag.* **2018**, *166*, 744–757. [CrossRef]
27. Pavan, K.N.; Chethan, K.S.; Suresh, R.B. Investigation on Heat Transfer Augmentation in Tubes with Rotating Twisted Tape Insert Using Water and Copper Oxide Nanofluid as Heat Transfer Medium. *J. Crit. Rev.* **2020**, *7*, 1595–1600.
28. Promvonge, P. Thermal Augmentation in Circular Tube with Twisted Tape and Wire Coil Turbulators. *Energy Convers. Manag.* **2008**, *49*, 2949–2955. [CrossRef]
29. Varun, K.; Arunachala, U.C.; Elton, D.N. Trade-off between Wire Matrix and Twisted Tape: SOLTRACE® Based Indoor Study of Parabolic Trough Collector. *Renew. Energy* **2020**, *156*, 478–492. [CrossRef]
30. Chakraborty, O.; Das, B.; Gupta, R. Impact of Helical Coil Insert in the Absorber Tube of Parabolic Trough Collector. *Smart Innov. Syst. Technol.* **2021**, *206*, 177–187. [CrossRef]
31. Zhao, Z.; Bai, F.; Zhang, X.; Wang, Z. Experimental Study of Pin Finned Receiver Tubes for a Parabolic Trough Solar Air Collector. *Sol. Energy* **2020**, *207*, 91–102. [CrossRef]
32. Jamal-Abad, M.T.; Saedodin, S.; Aminy, M. Experimental Investigation on a Solar Parabolic Trough Collector for Absorber Tube Filled with Porous Media. *Renew. Energy* **2017**, *107*, 156–163. [CrossRef]
33. Anand, S.C.; Rai, D.A.K.; Sachan, V. Comparative Study of Parabolic Trough Concentrators. *Int. J. Mech. Eng. Technol.* **2014**, *5*, 65–73.
34. Subramaniyan, C.; Subramani, J.; Kalidasan, B.; Anbuselvan, N.; Yuvaraj, T.; Prabaharan, N.; Senjyu, T. Investigation on the Optical Design and Performance of a Single-Axis-Tracking Solar Parabolic Trough Collector with a Secondary Reflector. *Sustainability* **2021**, *13*, 9918. [CrossRef]
35. Arasu, A.V.; Sornakumar, T. Design, Manufacture and Testing of Fiberglass Reinforced Parabola Trough for Parabolic Trough Solar Collectors. *Sol. Energy* **2007**, *81*, 1273–1279. [CrossRef]
36. Kalogirou, S.A. *Solar Energy Engineering: Processes and Systems*, 2nd ed.; Elsevier Inc.: Amsterdam, The Netherlands, 2014.
37. Büker, M.S.; Parlamış, H.; Alwetaishi, M.; Benjeddou, O. Experimental Investigation on the Dehumidification Performance of a Parabolic Trough Solar Air Collector Assisted Rotary Desiccant System. *Case Stud. Therm. Eng.* **2022**, *34*, 102077. [CrossRef]
38. Goodfellow Ceramic & Glass Division. *Properties of Borosilicate Glass*; Goodfellow Ceramic & Glass Division: Pittsburgh, PA, USA, 2009.
39. Reddy, K.S.; Ravi Kumar, K.; Ajay, C.S. Experimental Investigation of Porous Disc Enhanced Receiver for Solar Parabolic Trough Collector. *Renew. Energy* **2015**, *77*, 308–319. [CrossRef]
40. Romero-Alvarez, M.; Zarza, E. Handbook of Energy Efficiency and Renewable Energy. *Choice Rev. Online* **2008**, *45*, 45-2629. [CrossRef]
41. Ibrahim, E.Z. Augmentation of Laminar Flow and Heat Transfer in Flat Tubes by Means of Helical Screw-Tape Inserts. *Energy Convers. Manag.* **2011**, *52*, 250–257. [CrossRef]
42. Mwesigye, A.; Bello-Ochende, T.; Meyer, J.P. Heat Transfer and Thermodynamic Performance of a Parabolic Trough Receiver with Centrally Placed Perforated Plate Inserts. *Appl. Energy* **2014**, *136*, 989–1003. [CrossRef]
43. Eiamsa-ard, S.; Thianpong, C.; Eiamsa-ard, P. Turbulent Heat Transfer Enhancement by Counter/Co-Swirling Flow in a Tube Fitted with Twin Twisted Tapes. *Exp. Therm. Fluid Sci.* **2010**, *34*, 53–62. [CrossRef]
44. Chakraborty, O.; Das, B.; Gupta, R.; Debbarma, S. Heat Transfer Enhancement Analysis of Parabolic Trough Collector with Straight and Helical Absorber Tube. *Therm. Sci. Eng. Prog.* **2020**, *20*, 100718. [CrossRef]
45. Xiao, H.; Liu, P.; Liu, Z.; Liu, W. Performance Analyses in Parabolic Trough Collectors by Inserting Novel Inclined Curved-Twisted Baffles. *Renew. Energy* **2021**, *165*, 14–27. [CrossRef]
46. Kumar, B.N.; Reddy, K.S. Numerical Investigations on Metal Foam Inserted Solar Parabolic Trough DSG Absorber Tube for Mitigating Thermal Gradients and Enhancing Heat Transfer. *Appl. Therm. Eng.* **2020**, *178*, 115511. [CrossRef]
47. Bellos, E.; Tzivanidis, C. Investigation of a Star Flow Insert in a Parabolic Trough Solar Collector. *Appl. Energy* **2018**, *224*, 86–102. [CrossRef]
48. Bellos, E.; Tzivanidis, C.; Antonopoulos, K.A.; Gkinis, G. Thermal Enhancement of Solar Parabolic Trough Collectors by Using Nano Fl Uids and Converging-Diverging Absorber Tube. *Renew. Energy* **2016**, *94*, 213–222. [CrossRef]

49. Bozorg, M.V.; Hossein Doranehgard, M.; Hong, K.; Xiong, Q. CFD Study of Heat Transfer and Fluid Flow in a Parabolic Trough Solar Receiver with Internal Annular Porous Structure and Synthetic Oil–Al_2O_3 Nanofluid. *Renew. Energy* **2020**, *145*, 2598–2614. [CrossRef]
50. Vahidinia, F.; Khorasanizadeh, H.; Aghaei, A. Comparative Energy, Exergy and CO_2 Emission Evaluations of a LS-2 Parabolic Trough Solar Collector Using Al_2O_3/SiO_2-Syltherm 800 Hybrid Nanofluid. *Energy Convers. Manag.* **2021**, *245*, 114596. [CrossRef]
51. Bellos, E.; Tzivanidis, C.; Daniil, I.; Antonopoulos, K.A. The Impact of Internal Longitudinal Fins in Parabolic Trough Collectors Operating with Gases. *Energy Convers. Manag.* **2017**, *135*, 35–54. [CrossRef]
52. Akbarzadeh, S.; Valipour, M.S. Energy and Exergy Analysis of a Parabolic Trough Collector Using Helically Corrugated Absorber Tube. *Renew. Energy* **2020**, *155*, 735–747. [CrossRef]
53. Holman, J.P. *Experimental Methods for Engineers*, 8th ed.; McGraw-Hill Series in Mechanical Engineering: New York, NY, USA, 2011; Volume s1-VIII.
54. Kabeel, A.E.; Sharshir, S.W.; Abdelaziz, G.B.; Halim, M.A.; Swidan, A. Improving Performance of Tubular Solar Still by Controlling the Water Depth and Cover Cooling. *J. Clean. Prod.* **2019**, *233*, 848–856. [CrossRef]
55. Kumar, D.; Kumar, S. Thermal Performance of the Solar Parabolic Trough Collector at Different Flow Rates: An Experimental Study. *Int. J. Ambient Energy* **2018**, *39*, 93–102. [CrossRef]
56. Bellos, E.; Tzivanidis, C. Enhancing the Performance of a Parabolic Trough Collector with Combined Thermal and Optical Techniques. *Appl. Therm. Eng.* **2020**, *164*, 114496. [CrossRef]
57. Zheng, Z.; Xu, Y.; He, Y. Thermal Analysis of a Solar Parabolic Trough Receiver Tube with Porous Insert Optimized by Coupling Genetic Algorithm and CFD. *Sci. China Technol. Sci.* **2016**, *59*, 1475–1485. [CrossRef]
58. Ahmed, K.A.; Natarajan, E. Thermal Performance Enhancement in a Parabolic Trough Receiver Tube with Internal Toroidal Rings: A Numerical Investigation. *Appl. Therm. Eng.* **2019**, *162*, 114224. [CrossRef]
59. Bellos, E.; Tzivanidis, C. Enhancing the Performance of Evacuated and Non-Evacuated Parabolic Trough Collectors Using Twisted Tape Inserts, Perforated Plate Inserts and Internally Finned Absorber. *Energies* **2018**, *11*, 1129. [CrossRef]
60. Laaraba, A.; Mebarki, G. Enhancing Thermal Performance of a Parabolic Trough Collector with Inserting Longitudinal Fins in the Down Half of the Receiver Tube. *J. Therm. Sci.* **2020**, *29*, 1309–1321. [CrossRef]